Structural and Kinetic Studies on Native Intermediates and an Intermediate Analogue in Benzoylformate Decarboxylase Reveal a Least Motion Mechanism with an Unprecedented Short-Lived Predecarboxylation Intermediate‡

Marc Bruning,[§] Marco Berheide,[§] Danilo Meyer,[||,⊥] Ralph Golbik,[⊥] Hans Bartunik,[#] Andreas Liese,*[,§] and Kai Tittmann*[,||,⊥]

Institute of Technical Biocatalysis, Hamburg University of Technology, Denickestrasse 15, D-21073 Hamburg, Germany, Albrecht-von-Haller-Institute and Göttingen Center for Molecular Biosciences, Georg-August-University Göttingen, Ernst-Caspari-Haus, Justus-von-Liebig-Weg 11, D-37077 Göttingen, Germany, Institute of Biochemistry and Biotechnology, Martin-Luther-University Halle-Wittenberg, Kurt-Mothes-Strasse 3, D-06120 Halle/Saale, Germany, and Max-Planck-Gesellschaft, Arbeitsgruppen für strukturelle Molekularbiologie (MPG-ASMB) c/o DESY, Notkestrasse 85, D-22603 Hamburg, Germany

Received October 20, 2008; Revised Manuscript Received January 30, 2009

ABSTRACT: The thiamin diphosphate- (ThDP-) dependent enzyme benzoylformate decarboxylase (BFDC) catalyzes the nonoxidative decarboxylation of benzoylformic acid to benzaldehyde and carbon dioxide. To date, no structural information for a cofactor-bound reaction intermediate in BFDC is available. For kinetic analysis, a chromophoric substrate analogue was employed that produces various absorbing intermediates during turnover but is a poor substrate with a 10^4-fold compromised k_{cat}. Here, we have analyzed the steady-state distribution of native intermediates by a combined chemical quench/^{1}H NMR spectroscopic approach and estimated the net rate constants of elementary catalytic steps. At substrate saturation, carbonyl addition of the substrate to the cofactor ($k' \sim 500$ s^{-1} at 30 °C) and elimination of benzaldehyde ($k' \sim 2.400$ s^{-1}) were found to be partially rate-determining for catalysis, whereas decarboxylation of the transient 2-mandelyl-ThDP intermediate is 1 order of magnitude faster with $k' \sim 16.000$ s^{-1}, the largest rate constant of decarboxylation in any thiamin enzyme characterized so far. The X-ray structure of a predecarboxylation intermediate analogue was determined to 1.6 Å after cocrystallization of BFDC from *Pseudomonas putida* with benzoylphosphonic acid methyl ester. In contrast to the free acid, for which irreversible phosphorylation of active center Ser26 was reported, the methyl ester forms a covalent adduct with ThDP with a similar configuration at C2α as observed for other thiamin enzymes. The C2−C2α bond of the intermediate analogue is out of plane by 7°, indicating strain. The phosphonate part of the adduct forms hydrogen bonds with Ser26 and His281, and the 1-OH group is held in place by interactions with His70 and the 4′-amino group of ThDP. The phenyl ring accommodates in a hydrophobic pocket formed by Phe464, Phe397, Leu109, and Leu403. A comparison with the previously determined structure of BFDC in noncovalent complex with the inhibitor (*R*)-mandelate suggests a least motion mechanism. Binding of benzoylphosphonic acid methyl ester to BFDC was further characterized by CD spectroscopy and stopped-flow kinetics, indicating a two-step binding mechanism with a 200-fold slower carbonyl addition to ThDP than determined for benzoylformic acid, in line with the observed slight structural reorganization of Phe464 due to steric clashes with the phosphonate moiety.

The mandelate pathway allows several *Pseudomonas* species to use (*R*)-mandelic acid as a sole carbon source. The substrate (*R*)-mandelic acid is converted in a four-step reaction sequence to benzoic acid that subsequently enters the β-ketoadipate pathway (*1*−*6*). A key enzyme of the mandelate pathway is benzoylformate decarboxylase (BFDC,[1] EC 4.1.1.7) that carries out the nonoxidative transformation of benzoylformate (BF) to benzaldehyde and carbon dioxide (*7*).

The catalytic cycle of BFDC catalysis can be subdivided into several microscopic steps as proposed for other ThDP decarboxylases (Figure 1) (*8*). Initially, carbon 2 of the thiazolium is deprotonated, forming the reactive ylide form of the cofactor (step 0) (*9*). Next, the substrate BF binds to the active site (step 1), and the cofactor ylide attacks the

‡ The refined model and corresponding structure factor amplitudes have been deposited in the Research Collaboratory for Structural Biology (http://www.rcsb.org) under accession number 3FZN.

* To whom correspondence should be addressed. K.T.: phone, +49-551-3914430; fax, +49-551-395749; e-mail, ktittma@gwdg.de. A.L.: phone, +49-40-428783018; fax, +49-40-428782127; e-mail, liese@tuhh.de.

§ Hamburg University of Technology.

|| Georg-August-University Göttingen.

⊥ Martin-Luther-University Halle-Wittenberg.

Max-Planck-Gesellschaft.

[1] Abbreviations: BFDC, benzoylformate decarboxylase; BF, benzoylformate; NBF, *p*-nitro-BF; ThDP, thiamin diphosphate; MThDP, 2-mandelyl-ThDP; HBzThDP, 2-(1-hydroxybenzyl)-ThDP; MBP, methyl benzoylphosphonate; PMThDP, α-(methyl)phosphono-MThDP; PDC, pyruvate decarboxylase; LThDP, 2-lactyl-ThDP.

10.1021/bi801957d CCC: $40.75 © 2009 American Chemical Society
Published on Web 01/30/2009

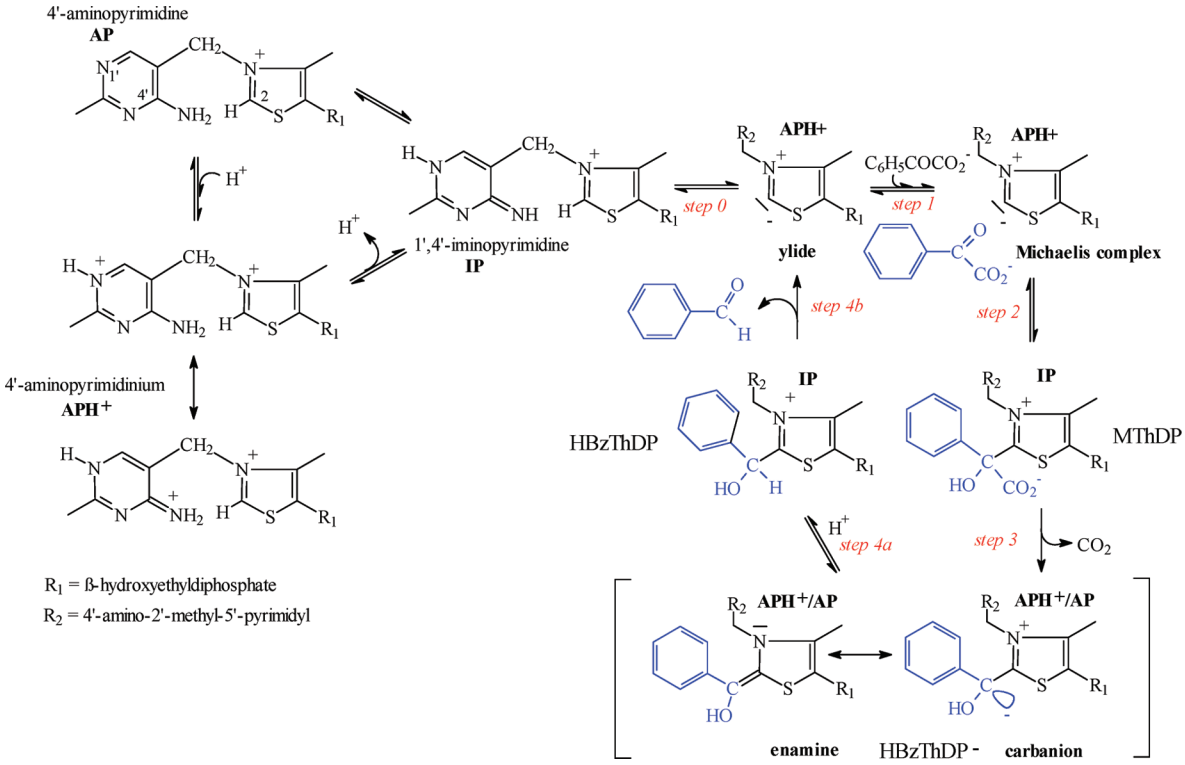

FIGURE 1: Catalytic cycle of BFDC with intermediates and elementary catalytic steps.

substrate carbonyl, yielding the tetrahedral adduct 2-mandelyl-ThDP (MThDP) (step 2). This intermediate decarboxylates (step 3) to the carbanion/enamine form of 2-(1-hydroxybenzyl)-ThDP (HBzThDP). Finally, liberation of benzaldehyde requires protonation of the carbanion/enamine (step 4a) at C2α and deprotonation of the α-hydroxyl group and cleavage of the C2−C2α bond (step 4b). According to model studies and CD spectroscopic data on other ThDP enzymes, the aminopyrimidine part of ThDP preferentially adopts the 1′,4′-imino tautomeric form (IP) in tetrahedral intermediates (BFDC: MThDP and HBzThDP), whereas the aminopyrimidine (AP) and aminopyrimidinium (APH^+) are predominantly formed at other stages of the catalytic cycle (*10, 11*). Noteworthy, the IP form gives rise to a positive CD spectral band centered around 300 nm, while a negative band at 330 nm is thought to pertain to an intramolecular charge transfer between AP and the thiazolium ring. So far, the APH^+ form in enzymes has escaped CD detection.

BFDC is a homotetramer with four identical active sites which are located at the dimer interface of two corresponding monomers (*12*). Except for the canonical *V* conformation of enzyme-bound ThDP and the conserved Glu residue that interacts with N1′ of the cofactor, the active site of BFDC differs substantially from those of related ThDP-dependent decarboxylases acting on nonaromatic 2-keto acids, e.g., pyruvate decarboxylases (PDC, EC 4.1.1.1) (*13, 14*). X-ray structural studies on BFDC in noncovalent complex with the inhibitor (*R*)-mandelate delineated a putative substrate binding mode (*15*). The structural data implicated catalytic roles for active center residues Ser26, His70, and His281. The suggested roles were corroborated in transient kinetic studies on wildtype BFDC and corresponding variants employing the chromophoric substrate analogue *p*-nitro-BF (NBF) that, upon addition to the enzyme, generates various absorbing intermediates including a short-lived intermediate at 600−620 nm assigned to be a charge-transfer complex of *p*-nitro-MThDP at the active site and a long-lived intermediate centered around 400 nm assigned to be the HBzThDP enamine intermediate (*16*). Although the band assignment conforms with the kinetic model and spectroscopic data on chemical models, an independent proof of the assignment made is missing so far. Also, despite fair affinity NBF is a very poor substrate of BFDC ($k_{cat} \sim 0.05\ s^{-1}$, $K_M \sim 0.15$ mM at 25 °C) compared to the native substrate BF ($k_{cat} \sim 450\ s^{-1}$, $K_M \sim 0.23$ mM at 30 °C), questioning the suitability of this conceptional framework for analyzing the reaction coordinate and individual energetic contributions of functional groups for transition state stabilization or reactant state destabilization. Furthermore, a detailed microscopic kinetic analysis for turnover of the native substrate BF is mandatory to explain how BFDC avoids fragmentation of the central HBzThDP carbanion/enamine intermediate observed in models (*17*).

The utilization of acyl phosphonates (the substrate carboxylate is replaced by a phosphonate or methylphosphonate) as electrostatic analogues of keto acid substrates turned out to be a successful approach for studying structure and function of ThDP enzymes (*18*). These analogues bind to C2 of enzyme-bound ThDP and form decarboxylation transition state analogues that are not further processed. The high-resolution X-ray structures of phosphonate-based predecarboxylation intermediate analogues were determined for pyruvate dehydrogenase E1 component, pyruvate oxidase, and benzaldehyde lyase (*19−21*). Remarkably, the addition of benzoylphosphonic acid to BFDC completely and irreversibly inactivated the enzyme by transfer of the phosphono group to active center Ser26 and formation of the phosphate ester (*22*).

Here, we have analyzed the steady-state distribution of covalent intermediates for turnover of the native substrate BF by ^{1}H NMR spectroscopy after chemical quench isolation (*23*) and correlate the estimated net rate constants of elementary catalytic steps with kinetic studies on models. In addition, the high-resolution X-ray structure of BFDC with a covalent adduct formed between ThDP and methyl benzoylphosphonate (MBP) is presented, and implications for the stereochemical course and putative catalytic roles of functional groups are discussed in the context of our current understanding of enzymic ThDP catalysis (*24*).

MATERIALS AND METHODS

Reagents. Horse liver alcohol dehydrogenase was from Roche Molecular Biochemical Inc. D_2O (99.9%), ThDP, and NADH were purchased from Sigma-Aldrich Chemie GmbH. All other chemicals were obtained from VWR International GmbH, Sigma-Aldrich Chemie GmbH, Carl Roth GmbH, and AppliChem GmbH. Quartz double-distilled water was used throughout the experiments.

Chemical Syntheses of p-Nitrobenzoylformate and Methyl Benzoylphosphonate. Synthesis of NBF was carried out by oxidation of *p*-nitroacetophenone by SeO_2 (*25*). MBP was synthesized in a similar way as described for methyl acetylphosphonate but using benzoyl chloride and trimethyl phosphite as reagents (*18*). Purity and correct synthesis of both compounds were confirmed by NMR spectroscopy and mass spectrometry.

Fermentation and Protein Purification. Escherichia coli SG13009 cells carrying the plasmid for BFDC-His_6 were cultivated by a substrate-limited fed-batch fermentation at 37 °C and using a Bioengineering 2 L foil fermenter. The media contained 200 mM potassium phosphate buffer, pH 7.1, supplemented with 4 mM NH_4Cl, 4 mM $MgSO_4$, 15 mM $(NH_4)_2SO_4$, 3 g/L yeast extract, 3 g/L glucose, and 0.1% (v/v) desmophen (an antifoam agent). After the addition of 0.5% (v/v) of trace element DSM 141 (200-fold stock) and vitamin DSM 141 solutions, antibiotics were added to a final concentration of 50 μg/mL kanamycin and 100 μg/mL ampicillin, respectively. After inoculation and batch phase, a feed solution was applied that contained 630 g/L glucose, 15 g/L yeast extract, and the vitamin/trace elements as mentioned before. The oxygen saturation was adjusted to 40% by varying the stirrer speed and by the aeration with compressed air and pure oxygen. At OD_{600} ~70 the culture was induced by adding IPTG to a final concentration of 1.5 mM, and the temperature was decreased to 28 °C. After 8 h cultivation time, cells were harvested at OD_{600} ~140 by centrifugation.

BFDC-His_6 was purified by metal ion affinity chromatography using a Ni-NTA column. Cells (40 g) were dissolved in 100 mL of disruption buffer (100 mM potassium phosphate buffer, pH 6.0, supplemented with 2 mM $MgCl_2$ and 0.5 mM ThDP). After treatment of the lysate with lysozyme (0.5 mg/mL final concentration) for 30 min the suspension was sonicated for 30 min using a 23 mm tip. After an additional centrifugation (75600*g*, 45 min) the cell free extract was applied to a Ni-NTA column (bed volume 75 mL) that was previously equilibrated with 100 mM potassium phosphate buffer, pH 7.0, supplemented with 0.1 mM ThDP and 2 mM $MgCl_2$. Proteins binding nonspecifically to the column were eluted with buffer containing 50 mM imidazole, and BFDC was eventually eluted by the same buffer but containing 250 mM imidazole at pH 7.5. The BFDC fractions were pooled and desalted by ultrafiltration using a 30 kDa membrane and disruption buffer. The solution was lyophilized, and the lyophilysate was stored at −20 °C.

Steady-State Assay. The activity of BFDC was determined in a coupled optical test employing NADH and horse liver alcohol dehydrogenase in 50 mM potassium phosphate buffer, pH 6.5, supplemented with 2.5 mM $MgSO_4$ and 200 μM ThDP at 30 °C as detailed in ref *8*. The catalytic constants were calculated by fitting the experimental data to the Michaelis−Menten equation.

Circular Dichroism Studies Using the Substrate Analogue Methyl Benzoylphosphonate. BFDC-catalyzed formation of α-(methyl)phosphono-mandelyl-ThDP (PMThDP, the covalent adduct between enzyme-bound ThDP and methyl benzoylphosphonate) was analyzed by CD spectroscopy using the positive signal of the cofactor IP form centered around 300 nm. CD spectra were recorded on a Jasco J-810 spectropolarimeter at 20 °C. BFDC lyophilysate was dissolved in 50 mM potassium phosphate buffer, pH 6.5, supplemented with 2.5 mM $MgSO_4$ and 200 μM ThDP. MBP as a sodium salt was dissolved in the same buffer and titrated to BFDC solution (2 mg/mL) up to a final concentration of 1.6 mM. CD spectra were recorded after a reaction time of 15 min in the 280−380 nm wavelength range with an optical path length of 10 mm. All spectra were corrected for buffer contributions. Difference spectra were calculated by subtraction with the CD spectrum of BFDC in the resting state. The apparent K_D for MBP was estimated using a hyperbolic function.

Steady-State Analysis of Reaction Intermediates by Chemical Quench/^{1}H NMR Spectroscopy. Prior to the chemical quench/NMR studies, BFDC lyophilysate was dissolved in 50 mM potassium phosphate buffer, pH 6.5 (supplemented with 2.5 mM $MgSO_4$), and desalted via a HiPrep column (GE Healthcare) to remove excess ThDP. It was established by activity measurements that the enzyme retains full activity in the absence of excess ThDP. BFDC was concentrated to a final concentration of 15 mg/mL corresponding to 267 μM active sites.

BFDC (15 mg/mL) was then mixed with 100 mM BF (in the same buffer) in 1 + 1 mixing ratio for different defined reaction times ranging from 5 to 5000 ms and using a rapid quench flow device (RQF-3; Kintek Althouse) as described before (*23*). The reaction was quenched by the addition of 1 volume of 12.5% (w/v) TCA and 1 M DCl (in D_2O). The denatured protein was discarded after centrifugation, and the supernatant containing the intermediates, substrates, and products was analyzed by ^{1}H NMR spectroscopy.

For the assignment and the quantitative analysis of ThDP, MThDP, and HBzThDP, the 2′-C**H**$_3$ and 4-C**H**$_3$ ^{1}H NMR singlet signals of ThDP (2.65 and 2.58 ppm), MThDP (2.50 and 2.41 ppm), and HBzThDP (2.47 and 2.42 ppm) were used. NMR aquisition and data processing were carried out as described previously (*8, 23*).

For the calculation of the unimolecular forward net rate constants of elementary steps of catalysis, a minimal catalytic scheme is assumed that comprises (i) the reversible, noncovalent binding of BF (K_1), (ii) the formation of MThDP (k'_2), (iii) the decarboxylation of MThDP (k'_3), and (iv) benzal-

dehyde release (k'_4). Noteworthy, the carbanion/enamine will be rapidly protonated at Cα after acid quench isolation, and the conjugate acid (HBzThDP) will be observed. Therefore and irrespective of a concerted or stepwise product release, k'_4 is a complex constant and reflects protonation of the carbanion/enamine, deprotonation of the α-hydroxyl group, and C2−C2α bond cleavage.

$$\text{E}-\text{ThDP} + \text{BF} \overset{K_1}{\rightleftharpoons} \text{E}-\text{ThDP}\cdot\text{BF} \quad \text{(Michaelis complex)} \tag{1}$$

$$\text{E}-\text{ThDP}\cdot\text{BF} \xrightarrow{k'_2} \text{E}-\text{MThDP} \tag{2}$$

$$\text{E}-\text{MThDP} \xrightarrow{k'_3} \text{E}-\text{HBzThDP carbanion/enamine (E}-\text{HBzThDP}^-) + \text{CO}_2 \tag{3}$$

$$\text{E}-\text{HBzThDP}^- + \text{H}^+ \xrightarrow{k'_4} \text{ThDP} + \text{benzaldehyde} \tag{4}$$

According to Cleland's transit time approach (*26*), k_{cat} can be defined as a function of the forward rate constants of single steps at substrate saturation as follows:

$$\frac{1}{k_{cat}} = \frac{1}{k'_2} + \frac{1}{k'_3} + \frac{1}{k'_4} \tag{5}$$

Since [S] ≫ K_M, the formation and decomposition of all enzymatic intermediates will be balanced at steady state. The steady-state intermediate concentration can be directly correlated with the net rate constants of catalysis as follows:

$$\frac{[\text{E}-\text{MThDP}]}{[\text{E}-\text{ThDP}]} = \frac{k'_2}{k'_3} = a \tag{6}$$

$$\frac{[\text{E}-\text{HBzThDP}]}{[\text{E}-\text{MThDP}]} = \frac{k'_3}{k'_4} = b \tag{7}$$

The fraction of isolated cofactor as unsubstituted ThDP was corrected for nonsaturation of the enzyme with substrate according to the Michaelis−Menten equation. Due to the nonenzymic decarboxylation of MThDP after acid quench isolation (k_{obs} = 3.1 × 10^{-4} s^{-1} at pH 0.75 and 25 °C) the intermediate concentrations were corrected for this decomposition as previously described (*8*). Using the corrected steady-state intermediate distribution, k_{cat}, and eqs 8−10, the net rate constants of elementary catalytic steps were derived:

$$k'_2 = k_{cat}(1 + a + ab) \tag{8}$$

$$k'_3 = k_{cat}\frac{(1 + a + ab)}{a} \tag{9}$$

$$k'_4 = k_{cat}\frac{(1 + a + ab)}{ab} \tag{10}$$

Analysis of p-Nitro-BF Turnover and Methyl Benzoylphosphonate Binding to BFDC by Stopped-Flow Kinetics and NMR Spectroscopy. BFDC-catalyzed turnover of the chromophoric substrate analogue NBF by BFDC was analyzed by stopped-flow kinetics as reported in ref *16*. BFDC (4.8 mg/mL in 50 mM potassium phosphate buffer, pH 6.5, and 2.5 mM $MgSO_4$) was mixed with 10 mM NBF (same buffer) in 1 + 1 mixing ratio at 20 °C on a SX.18MV device from Applied Photophysics (Leatherhead, U.K.). Transients were recorded at 400 and 600 nm and subjected to kinetic analysis using the programs Sigma Plot and KaleidaGraph. NMR-based analysis of reaction intermediates after chemical quench isolation was carried out under identical condition but employing 15 mg/mL BFDC. Reaction times were inferred from the stopped-flow transients (see Results section). Chemical quenching, NMR data acquisition, and analysis were conducted as described in the NMR part of the Materials and Methods section.

Reaction of BFDC with substrate analogue MBP was analyzed by absorption stopped-flow kinetics at 308 nm, where the 1′,4′-imino tautomeric form of enzyme-bound ThDP/ThDP adducts gives rise to an absorbance signal. BFDC (2 or 15 mg/mL in 50 mM potassium phosphate buffer, pH 6.5, 200 μM ThDP, 2.5 mM $MgSO_4$) was reacted with MBP sodium salt (dissolved in the same buffer) of different concentration (up to 20 mM) in 1 + 1 mixing ratio at 30 °C. Transients were analyzed using SigmaPlot and KaleidaGraph. Formation of PMThDP under identical reaction conditions was analyzed by ^{1}H NMR spectroscopy after acid quench isolation as detailed before.

Protein Crystallization, Data Collection, and Structure Determination. BFDC lyophilysate was dissolved to a protein concentration of 20 mg/mL in 20 mM Tris-HCl buffer, pH 7.4, and subsequently crystallized in the presence of 100 mM MBP using the sitting vapor drop diffusion method against a reservoir solution containing 25% (w/v) polyethylene glycol 2000 and 0.2 M $MgCl_2$ at pH 6.1 (adjusted by a mixture of 0.5 M sodium acetate, 0.5 M glycylglycine, and 0.5 M Bis-Tris buffered at pH 4.5 and pH 9.0, respectively). Crystallization conditions are notably different from those reported in previous structural studies on BFDC from *Pseudomonas putida*, where either calcium chloride (unliganded resting state) or ammonium sulfate (complex with inhibitor (*R*)-mandelate) was added as coprecipitants (*15, 27*).

An X-ray data set of BFDC in complex with MBP was collected from a single crystal using Beamline BW6, Max-Planck Gesellschaft, Deutsches Elektronen Synchrotron, Hamburg. A total of 600 images were collected over an angular range of 150° with a ϕ slicing of 0.25°. The exposure time amounted for ∼4.6 h with an average dose of 2300 counts per image. BFDC crystals were looped directly from the mother liquor, flash-cooled in 100 K nitrogen stream, and mounted to the goniometer head. No additional cryoprotectants were added. The diffraction data extended to a resolution of 1.62 Å.

Processing of the crystallographic data sets was carried out with Denzo/Scalepack (*28*). Initial phases for modeling the BFD tetramer were obtained from molecular replacement phasing using Molrep (*29*) with the monomer of *P. putida* BFDC (PDB code 1mcz) as a search model. BFDC in complex with MBP crystallized in space group *P*1 with four monomers (a functional tetramer) in the crystallographic asymmetric unit. Inspection of electron density maps, model building, and refinement until eventual convergence of the free *R*-factor and the crystallographic *R*-factor were conducted with Refmac5 (*30*) and Coot (*31*).

While initial and simulated annealing omit maps unambiguously suggest a covalent adduct of ThDP and MBP (Supporting

Information Figure 1), initial refinement trials were carried out solely with ThDP bound to the active site while the MBP moiety was explicitly not modeled. However, at a late stage of refinement, due to the strong continuous electron density connecting the ThDP and benzoylphosphonate moieties a covalent adduct of the two ligands was added to the active sites of the BFDC tetramer. The initial PMThDP adduct was regularized and energy minimized to give a correctly sp^3-hybridized C2α carbon covalently linked to C2 of ThDP. For modeling of the PMThDP adduct, the structure was generated in the CCP4 monomer library sketcher. The library description was generated in CIF format using Libcheck of the CCP4 suite (*30*). The C2α atom of PMThDP was defined to be in plane with the planar thiazolium portion as an opposing restraint to out-of-plane deviation of the C2−C2α bond during crystallographic refinement. Multiple refinement cycles with the covalent complex did not reveal any difference density for the C2−C2α bond, thus clearly confirming the presence of a covalent adduct in the crystal. The average *B*-factors of all four PMThDP adducts are almost similar to that of nearby side chains (<5 Å distance), indicating full occupancy of the intermediate (*B*-factors in Å^2 for adduct/side chains: 16.8/16.7, 16.5/16.3, 17.2/17.1, and 17.6/17.6). However, the *B*-factors of the phosphonate moieties of the PMThDP adducts are slightly higher in comparison to those of the phenyl ring and of the ThDP part, indicating minor radiation damage (dephosphorylation) resulting from the data collection process. As a consequence of the presumably slightly lower occupancy of the phosphonate moiety, the electron density along the C2α−P bond of PMThDP is somewhat weaker relative to other portions of the adduct (see Results section). That notwithstanding, all four ligands were modeled with full occupancy in the BFDC tetramer with the phosphonate groups showing only slightly elevated *B*-factors in good accordance with the rest of the model. The final geometry of PMThDP corresponds very well with the observed electron density. Crystallographic statistics are detailed in Table 1. Crystallographic figures were prepared with Pymol (W. L. DeLano, DeLano Scientific, San Carlos, CA (http://www.pymol.org/)).

Table 1: X-ray Crystallographic Statistics[a]

Data Collection	
wavelength (Å)	1.05
space group	*P*1
cell dimensions (Å)	$a = 71.5$, $b = 93.3$, $c = 94.5$
cell dimensions (deg)	$\alpha = 63$, $\beta = 72$, $\gamma = 73$
resolution range (Å)	20.00−1.62 (1.64−1.62)
no. of observations	445901
no. of unique reflections	243335
completeness (%)	93.2 (92.3)
$\langle I/\sigma(I)\rangle$	8.2 (2.1)
R_{merge} (%)	10.7 (39.0)
redundancy	1.83 (1.82)
fraction of reflections observed once (%)	15.6 (16.5)
B-factor from Wilson plot (Å^2)	21.5
Refinement	
resolution range (Å)	19.96−1.62
reflections (working/test)	230330/12259
R_{cryst}/R_{free} (%)	17.0/20.3
mean *B*-factor (Å^2)	14.4
B-factor of intermediate (Å^2)	
residue 601/602/603/604	16.8/16.5/17.2/17.6
non-hydrogen atoms	18502
water molecules	2217
rms bond length deviation (Å)	0.016
rms bond angle deviation (deg)	1.481
Ramachandran analysis	
most favored (%)	92.9
allowed (%)	6.9

[a] $R_{merge} = \sum|I - \langle I\rangle|/\sum\langle I\rangle$. Values in parentheses correspond to the highest resolution shell. $R_{cryst} = \sum||F_o| - |F_c||/\sum|F_o|$. R_{free} is calculated as for R_{cryst} but for a test set comprising reflections not used in the refinement (5.0%).

RESULTS

BFDC was purified to homogeneity by affinity chromatography, and the estimated steady-state kinetic constants (K_M(BF) = 0.23 ± 0.02 mM, k_{cat} = 426 ± 6 s^{-1} at 30 °C and pH 6.5) determined in a coupled optical assay are in good agreement with the literature (K_M(BF) = 0.37 ± 0.02 mM, k_{cat} = 241 ± 4 s^{-1} at 20 °C and pH 7.0) (*15*).

Analysis of BFDC-Catalyzed Conversion of Chromophoric Substrate Analogue p-Nitro-BF by Stopped-Flow Kinetics and NMR Spectroscopy. Sergienko et al. reported that NBF was slowly converted by BFDC (k_{cat} ~0.05 s^{-1} at 25 °C), and its addition to the enzyme resulted in the formation of various absorbing intermediates (*16*). A transient intermediate at 600−620 nm (denoted as I_1) was assigned to *p*-nitro-MThDP forming a charge-transfer complex at the active site, whereas a long-lived intermediate with an absorbance maximum at 400−410 nm (denoted as I_2) was suggested to pertain to the enamine form of *p*-nitro-HBzThDP. We could qualitatively reproduce the stopped-flow kinetic data reported in ref *16*. After addition of 5 mM *p*-nitro-BF to BFDC at 20 °C and pH 6.5, transient I_1 at 600 nm is formed with a rate constant of k_1^{600} = 101 s^{-1} and depleted with k_2^{600} = 14.7 s^{-1} (Figure 2). Formation of I_2 at 400 nm is a two-step process with first-order rate constants of k_1^{400} = 15.5 s^{-1} (paralleling the rate of depletion of I_1) and k_2^{400} = 1.2 s^{-1}.

In order to assign I_1 and I_2 and the different rate constants, the intermediates formed upon addition of NBF to BFDC were isolated by acid quench after 20 ms (maximal concentration of I_1), 200 ms (almost complete depletion of I_1), and 5 s (maximal concentration of I_2, steady-state established) and subjected to ^{1}H NMR spectroscopic analysis. If the assignment proposed in ref *16* is correct, according to eq 11 approximately 71% of all active centers should be occupied with the *p*-nitro-MThDP intermediate at 20 ms under the chosen experimental conditions. Decarboxylation of *p*-nitro-MThDP should then result in the buildup of *p*-nitro-HBzThDP.

$$\frac{[NO_2-MThDP]_{max}}{[\text{active sites}]_{total}} = (k_1^{600}/k_2^{600})^{-k_2^{600}/(k_1^{600}-k_2^{600})} \quad (11)$$

Quantitative NMR analysis of the 4-C**H**$_3$ and 2′-C**H**$_3$ methyl singlets of ThDP/ThDP adducts reveals, however, that after 20 ms, 92% of all active sites contain C2-unsubstituted ThDP and 8% contain the *p*-nitro-HBzThDP intermediate that could be unambigously assigned via its C2α-**H** singlet at 6.17 ppm, the C6′-**H** singlet at 6.69 ppm, and the multiplet signal of the aromatic protons from the *p*-nitrobenzoyl moiety at 7.5 ppm. After 200 ms reaction time approximately 30% of the active sites contain nitro-HBzThDP, and the persistent steady-state concentration of it amounts for even ~70% active site total (at 5 s), clearly confirming I_2 to be the long-lived HBzThDP intermediate, presumably in the enamine form. Although *p*-nitro-MThDP

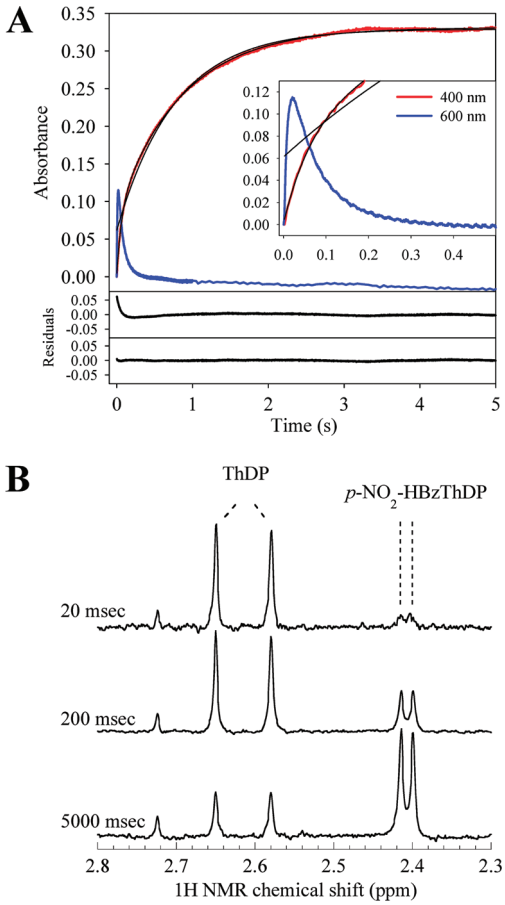

FIGURE 2: Analysis of BFDC-catalyzed turnover of chromophoric substrate analogue NBF by absorbance stopped-flow kinetics (A) and acid quench/NMR spectroscopy (B). (A) BFDC (2.4 mg/mL) was reacted with 5 mM NBF in 50 mM potassium phosphate and 2.5 mM $MgSO_4$ at 20 °C in a stopped-flow instrument. Transients were recorded at 400 nm (red) and 600 nm (blue) and fitted to monoexponential and double-exponential functions, respectively. Exemplified for the transient at 400 nm, the individual fit residuals are given below (single exponential, upper panel; double exponential, lower panel). (B) ^{1}H NMR spectra of acid quench isolated intermediates after 20, 200, and 5000 ms reaction time of BFDC and NBF showing the methyl fingerprint region (2′-CH_3 and 4-CH_3 singlets) of ThDP and ThDP adducts.

will slowly decarboxylate after acid quench isolation (MThDP decarboxylates with $t_{1/2}$ ~40 min), the inability to detect even traces of it makes it unlikely that I_1 is the covalent nitro-MThDP adduct. Even if the material would immediately decarboxylate after acid quench isolation (an unlikely prospect in view of the lifetime of MThDP), a larger fraction of the nitro-HBzThDP adduct should have been detected. We thus suggest to assign I_1 to the substrate Michaelis complex rather than the covalent predecarboxylation intermediate. This new assignment would have immediate consequences for the kinetic assignment of the different phases. Buildup of I_1 (k_1^{600}) would correspond to Michaelis complex formation; depletion of I_1/buildup of I_2 (k_2^{600}, k_1^{400}) would, in a kinetic sense, reflect all steps from the Michaelis complex until formation of the enamine. As there is no MThDP detectable, the observed rate constant mainly reflects carbonyl addition of the substrate to the cofactor rather than decarboxylation as suggested earlier (*15, 16*). Decarboxylation thus appears to be much faster than Michaelis complex formation and carbonyl addition.

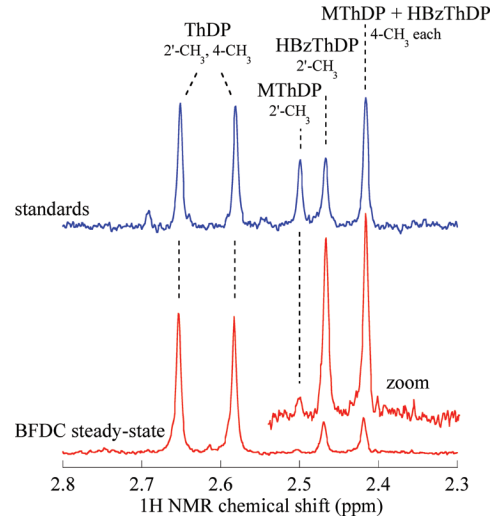

FIGURE 3: Steady-state intermediate distribution of covalent intermediates in the nonoxidative decarboxylation of BF by BFDC wild type. The intermediates were isolated by acid quench after a reaction time of 100 ms in 50 mM potassium phosphate buffer and 2.5 mM $MgSO_4$, pH 6.5 at 30 °C, and analyzed by ^{1}H NMR at pH 0.75 using the chemical shifts of the 2′-CH_3 and 4-CH_3 singlets of ThDP, MThDP, and HBzThDP.

Intermediate Distribution of BFDC at Steady State. The distribution of covalent reaction intermediates of BFDC at steady state during turnover of the native substrate BF was analyzed by ^{1}H NMR spectroscopy after acid quench isolation at different time points ranging from 5 ms until a few seconds (*23*). Due to the high enzyme concentration needed for the NMR-based analysis, the true steady state with stable intermediate fractions persists only until 200 ms, and different intermediate patterns are observed at longer reaction times (data not shown). A representative steady-state intermediate distribution after 100 ms reaction time is shown in Figure 3. The analysis reveals that approximately 79% of the active sites contain C2-unsubstituted ThDP and 18% are occupied with HBzThDP and 3% with MThDP (after correction for nonenzymic decarboxylation of MThDP after acid quench isolation). The 2′-CH_3 signal of quench-isolated MThDP is at the limit of resolution (signal-to-noise ratio ~3−4) but can be properly resolved. In line with this, the difference in intensity of the signal at 2.41−2.42 ppm (the 4-CH_3 signals of MThDP *and* HBzThDP) and that at 2.47 ppm (the 2′-CH_3 signal of HBzThDP) equals the relative intensity of the 2′-CH_3 signal of MThDP at 2.50 ppm.

Taking into account the catalytic constant of BFDC under the chosen experimental conditions (k_{cat} = 426 s^{-1}), the net rate constants of elementary steps can be estimated according to eqs 5−10. The analysis reveals the carbonyl addition of BF from a docking site to C2 of ThDP to be rate-determining for BFDC catalysis (k'_2 = 536 s^{-1}), whereas decarboxylation of MThDP (k'_3 = 16.460 s^{-1}) and elimination of benzaldehyde (k'_4 = 2.376 s^{-1}) proceed at least 1 order of magnitude faster. In fact, decarboxylation of MThDP in BFDC is much faster than decarboxylation of the corresponding 2-lactyl-ThDP (LThDP) intermediate in enzymes acting on pyruvate (*23, 32, 33*). Here, rate constants of ~200−500 s^{-1} were estimated for decarboxylation under comparable conditions as employed for BFDC.

Circular Dichroism Studies Using the Substrate Analogue Methyl Benzoylphosphonate. In the resting state, the near-

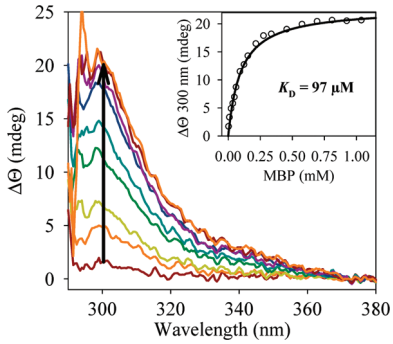

FIGURE 4: Near-UV circular dichroism difference spectra obtained after addition of increasing amounts of BF analogue MBP (0−1.6 mM) to 2 mg/mL BFDC in 0.1 M potassium phosphate, pH 6.5, supplemented with 2.5 mM $MgSO_4$ and 200 μM ThDP at 20 °C. Inset: The analysis of the dependence of the CD signal intensity at 300 nm on the MBP concentration was fitted to a hyperbolic function and yielded an apparent dissociation constant of 97 ± 9 μM.

UV CD spectrum of BFDC suggests that enzyme-bound ThDP is in part stabilized in the IP form as evidenced by the positive signal at 300−310 nm (Supporting Information Figure 2). There is no indication for the AP form, for which a negative CD signal at 320−330 would be expected. Addition of MBP to BFDC results in a concentration-dependent hyperbolic increase of the IP signal at 300 nm, yielding an apparent dissociation constant of 97 ± 9 μM (Figure 4 and Supporting Information Figure 2).

Kinetics of Methyl Benzoylphosphonate Binding by Stopped-Flow Kinetics and Acid Quench/NMR Spectroscopy. Kinetics of MBP binding to BFDC were analyzed by absorbance stopped-flow measurements at 308 nm using the intrinsic absorbance of the cofactor's IP form that is stabilized after formation of the covalent PMThDP adduct. The stopped-flow transients recorded after mixing of BFDC with different MBP concentrations cannot be fitted to a single-exponential function but rather to a double-exponential function (Figure 5). Plotting of the rate constants versus MBP concentration reveals a linear dependence for one rate constant (k_{obs}^1) and a hyperbolic dependence for the other (k_{obs}^2), implying a kinetic two-step mechanism with transient formation of a Michaelis complex.

$$\text{E−ThDP} + \text{MBP} \underset{k_{-1}}{\overset{k_{+1}}{\rightleftharpoons}} \text{E−ThDP·MBP} \quad \text{(Michaelis complex)} \tag{12}$$

$$\text{E−ThDP·MBP} \underset{k_{-2}}{\overset{k_{+2}}{\rightleftharpoons}} \text{E−α-(methyl)phosphonomandelyl-ThDP} \tag{13}$$

The dependence of k_{obs}^1 and k_{obs}^2 on the MBP concentration was fitted according to eqs 14−16:

$$k_{obs}^1 = k_{+1}[\text{MBP}] + k_{-1} \tag{14}$$

$$k_{obs}^2 = k_{-2} + \frac{k_{+2}[\text{MBP}]}{K_1 + [\text{MBP}]} \tag{15}$$

with

$$K_1 = \frac{k_{-1}}{k_{+1}} \tag{16}$$

and yielded rate constants of $k_{+1} = (6.34 \pm 1.18) \times 10^3$ M^{-1} s^{-1}, $k_{-1} = 13.5 \pm 1.1$ s^{-1}, $k_{+2} = 2.33 \pm 0.17$ s^{-1}, and $k_{-2} = 0.33 \pm 0.12$ s^{-1} and an equilibrium constant $K_1 = 325 \pm 104$ μM.

Concomitant analysis of reaction intermediates by NMR spectroscopy after acid quench isolation confirms that the slow phase seen in the stopped-flow experiments correlates with formation of the covalent PMThDP adduct (Supporting Information Figure 3).

Structure of a Predecarboxylation Intermediate Analogue at the Active Site of BFDC. BFDC was successfully cocrystallized with MBP, an electrostatic analogue of the native substrate BF. The X-ray structure of BFDC in complex with MBP was solved by molecular replacement phasing against data to 1.60 Å (Table 1). Unlike benzoylphosphonate that irreversibly inactivated the enzyme by phosphorylation of active center Ser26 (*22*), the methyl ester did bind to C2 of ThDP in a stable form, yielding the covalent predecarboxylation analogue α-(methyl)phosphonomandelyl-ThDP (Figure 6). The configuration at C2α is identical to these of related tetrahedral thiamin intermediates such as LThDP in pyruvate oxidase or pyruvate dehydrogenase (*19, 20*) and X5P-ThDP (the covalent adduct of ThDP and D-xylulose 5-phosphate) in transketolase (*34*). The phosphonate part is directed perpendicular to the thiazolium ring plane, and the α-OH group is forming a hydrogen bond with N4′ of the aminopyrimidine part of the cofactor. The native intermediate MThDP will thus be formed as the *S*-enantiomer in BFDC. The C2−C2α bond connecting C2 of ThDP and C2 of MBP is slightly out of the aromatic thiazolium ring plane (~7°) even when applying opposing restraints during refinement. A relaxation of the in-plane restraints resulted in a more pronounced deviation from coplanarity of the C2−C2α bond: the C5−S1−C2−C2α torsion angle increased up to 19° with fully relaxed restraints. An out-of-plane distortion of the C2−C2α bond appears to be a conserved structural feature of almost every tetrahedral thiamin intermediate that has been characterized so far, although distortion from planarity varies from 7° in POX to 25° in transketolase (*20, 34*).

Two oxygen atoms of the phosphonate moiety form hydrogen bonds with Ser26 and His281, and His70 interacts with N4′ and α-OH of the adduct. The substrate-specific phenyl ring accommodates in a hydrophobic pocket consisting of Leu109, Phe397, Leu403, and Phe464 (Supporting Information Figure 4).

A superposition of the newly determined structure with that of BFDC in complex with the inhibitor (*R*)-mandelate (*15*) reveals that all atoms of the benzoylphosphonate moiety except for C2α occupy almost identical positions as the corresponding atoms of (*R*)-mandelate (Figure 7). The same holds true for the spatial coordinates of most active site residues. The only major difference is detectable for the side chain of Phe464 (in three of four subunits) as a consequence of steric clashes of the phenyl ring with the methoxy group of the phosphonate (Figure 7).

DISCUSSION

Within the family of ThDP-dependent decarboxylases, BFDC exhibits some unique structural and catalytic features

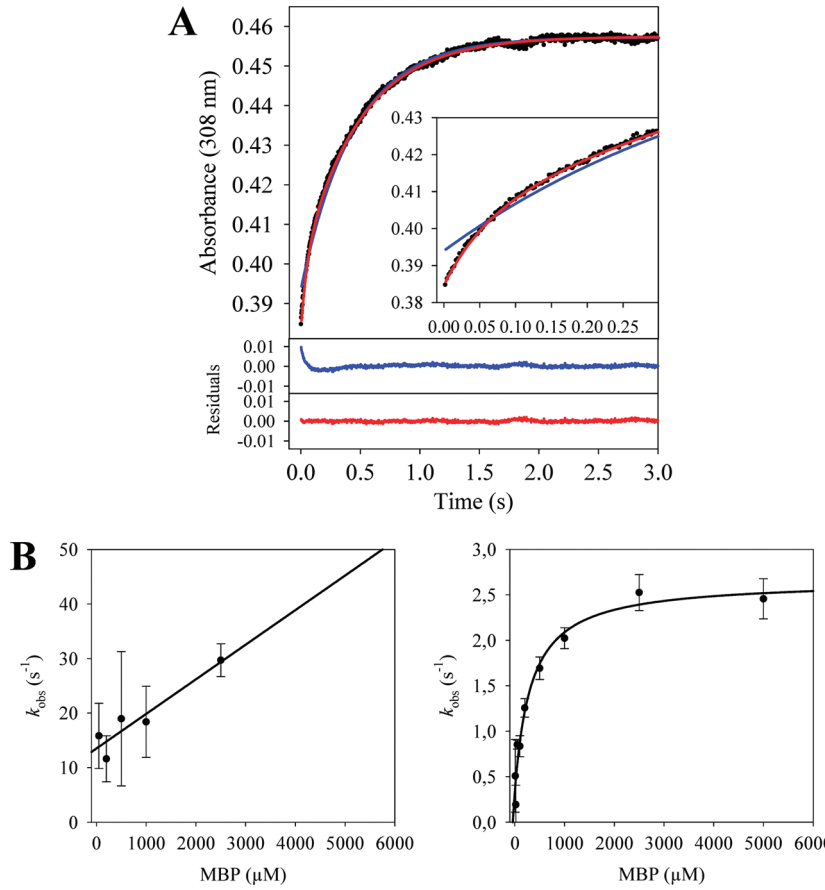

FIGURE 5: Analysis of MBP binding to BFDC by stopped-flow kinetics. (A) Transient recorded at 308 nm after mixing of 1 mg/mL BFDC with 1 mM MBP in 50 mM potassium phosphate buffer (supplemented with 2.5 mM $MgSO_4$ and 200 μM ThDP) at 30 °C. The progress curve was fitted to a monoexponential (blue) and double-exponential (red) function. Individual fit residuals are shown below. (B) Dependence of the observed rate constants obtained in (A) on MBP concentration.

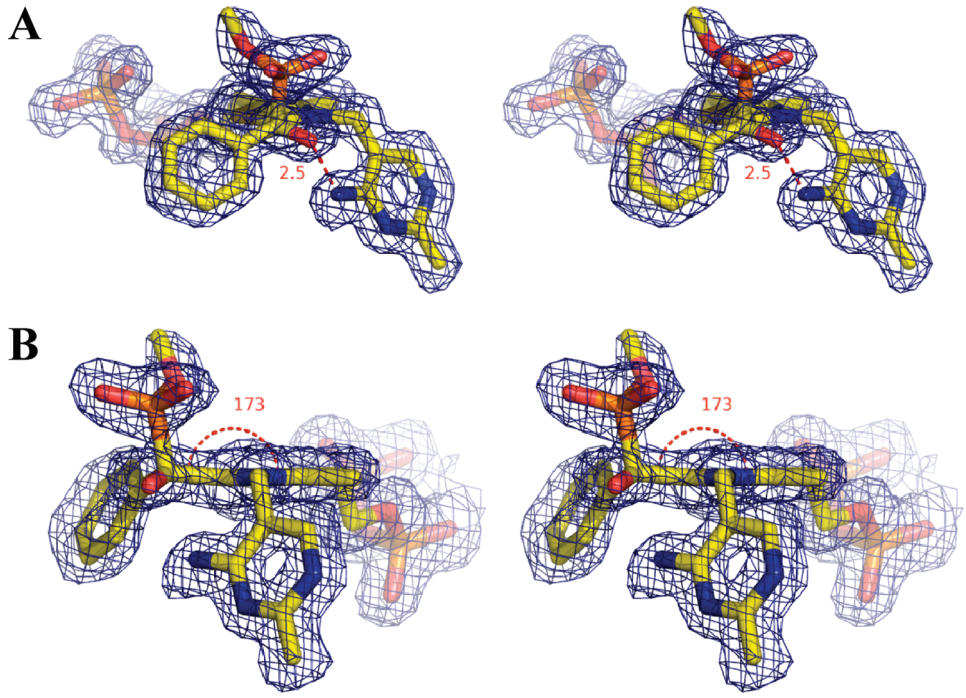

FIGURE 6: X-ray structure of predecarboxylation intermediate analogue α-(methyl)phosphono-MThDP at the active center of BFDC in stereoview. The electron density is contoured at 1.0σ in a $2F_o - F_c$ map. The adduct is shown in different orientations, and the interatomic distance between N4′ and α-OH (A) and the dihedral angle C5−S1−C2−C2α (B) are indicated. The electron density map was calculated from model phases of a model after inclusion of the MBP moiety of the PMThDP adduct.

(*12*). Apart from the canonical *V* conformation of enzyme-bound ThDP, the active site architecture of BFDC differs substantially from those of related enzymes converting aliphatic keto acids (pyruvate decarboxylase, branched-chain

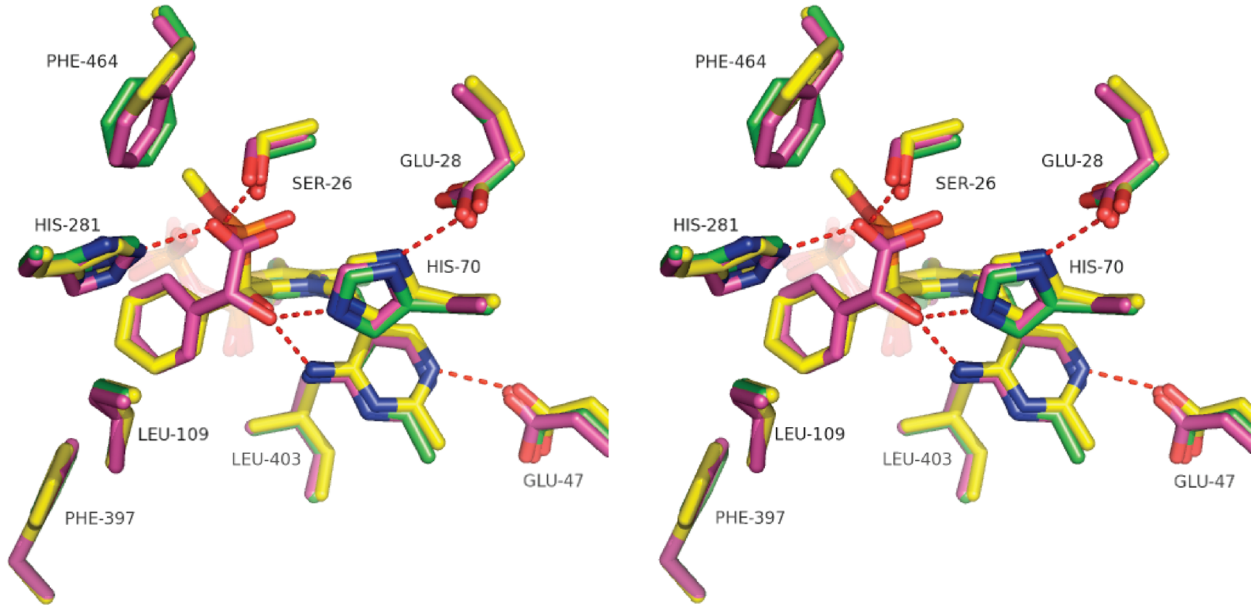

FIGURE 7: Superposition of the active site of BFDC in different states: resting state (green), in noncovalent complex with inhibitor (*R*)-mandelate (pink), and in complex with predecarboxylation intermediate analogue PMThDP (yellow). Dotted lines indicate hydrogen-bonding interactions (<3 Å contacts) between PMThDP and the enzyme.

keto acid decarboxylase) or aromatic keto acids (indolepyruvate decarboxylase, phenylpyruvate decarboxylase) (*13, 14, 35*−*37*). Despite small variations, these enzymes share a common substrate binding motif suggesting a conserved mechanism (*24*). On the basis of structural and kinetic studies on BFDC wild type and variants, the active center residues Ser26, His281, and His70 were implicated to be key players for catalysis and substrate binding (*15*), although a recent saturation mutagenesis study on BFDC has put into question the suggested catalytic roles since replacement of the three residues by amino acids incapable of acting as acid/base catalysts or hydrogen bond donor/acceptors had only moderate effects on catalysis (*38*). Most remarkably, these studies suggested that His281 is not an essential acid/base catalyst, although it would be suitably positioned to protonate the HBzThDP carbanion/enamine intermediate. Sequence alignment of BFDCs from different species showed that His281 is not invariant and may be replaced by Ser, Tyr, and Thr (*38*). This poses an immediate question about the mechanism of protonation and the acid/base catalyst involved.

A difficult chemical challenge BFDC has met with success is to avoid fragmentation of the HBzThDP carbanion/enamine intermediate, an unimolecular reaction that proceeds extremely fast in models ($k \sim 10^4$ s^{-1} at 40 °C) (*17, 24*) when compared to the overall reaction of BFDC ($k_{cat} = 4.3 \times 10^2$ s^{-1} at 30 °C). There is no evidence for this reaction taking place at the active center of BFDC. How does BFDC suppress this abortive side reaction?

In the current kinetic and structural study, we have attempted to address some of these open questions. The NMR-based analysis of intermediates at steady state during turnover of its native substrate BF revealed that formation of the initial tetrahedral MThDP intermediate and release of benzaldehyde from HBzThDP are rate-determining for overall catalysis, whereas the kinetic significance of the decarboxylation reaction is much lower than predicted by ^{13}C isotope effect studies (*39*) as just ~3% of all active sites contain predecarboxylation intermediate. According to the Albery-Knowles concept an energetic leveling of enzymic reactant states and transition states (termed "matched internal thermodynamics") has evolved as an inevitable consequence of enzyme evolution (*40*). In accordance with this concept, similar kinetic barriers were estimated for microscopic catalytic steps in other ThDP enzymes carrying out oxidative and nonoxidative decarboxylation of keto acids, and comparable fractions of pre- and postdecarboxylation intermediates were observed in these enzymes under turnover conditions (*23, 32, 33*). In BFDC, the predecarboxylation intermediate is extremely short-lived compared to other intermediates. Decarboxylation proceeds with 16000 s^{-1} at 30 °C, thus exceeding the rate of decarboxylation in all other ThDP decarboxylases by 2 orders of magnitude or more. Kluger's work on chemical models suggested that decarboxylation of thiamin adducts in decarboxylases is catalyzed by preassociated acids that protonate the carbanion formed upon decarboxylation, thus preventing recombination of CO_2 with the carbanion (*41*). In that way, the internal return of CO_2 is overcome, and it can diffuse out of the active site. Considering this principle, forward commitment of decarboxylation (separation of the CO_2/carbanion pair by protonation) in ThDP decarboxylase will, among other factors, critically depend on the rates of Cα protonation, C−C recombination, and diffusion. Since diffusion of CO_2 (~10^8 s^{-1}) is considered to be much slower than the barrierless recombination of CO_2 and a carbanion (~10^{13} s^{-1}), protonation of a built-in acid/base catalyst is mandatory to promote forward commitment by blocking return of CO_2 (*24*). The rapid decarboxylation in BFDC may thus reflect rapid trapping of the carbanion/enamine by protonation, the upper rate limit of which could equal the estimated rate of decarboxylation. If indeed protonation of the carbanion/enamine was to drive decarboxylation and proceeds that rapidly (~1.6×10^4 s^{-1} at 30 °C, ~$3-5 \times 10^4$ s^{-1} at 40 °C), it could successfully compete with fragmentation of the HBzThDP carbanion/enamine (~1×10^4 s^{-1} at 40 °C in models), providing a rationale for the suppressed fragmenta-

tion on the enzyme. That notwithstanding, the question remains why protonation of the HBzThDP carbanion/enamine would proceed that rapidly in BFDC compared to other ThDP decarboxylases. Structural comparison of a newly determined X-ray structure of BFDC with a phosphonate-based predecarboxylation intermediate analogue with a previously determined structure of BFDC in complex with inhibitor (*R*)-mandelate suggests a least motion mechanism for BFDC. Except for C2α, all atoms of PMThDP deriving from MBP superpose with the equivalent atoms of the inhibitor, the binding mode of which serves as a fair model for that of the substrate BF. It may thus be concluded that addition of BF to C2 of ThDP would just require hybridization of the substrate carbonyl from sp^2 to sp^3 without further structural rearrangements. Subsequent decarboxylation of the resulting MThDP intermediate is facilitated by (i) the perpendicular orientation of the carboxylate leaving group in terms of a maximum overlap mechanism as suggested for other ThDP enzymes (*24*), (ii) intramolecular strain of the adduct (7° deviation from planarity of the C2−C2α bond), and (iii) rapid trapping of the carbanion/enamine by protonation, presumably occurring in the transition state of decarboxylation. It seems likely that the binding mode of the substrate enforces a tetrahedral conformation for covalent intermediates throughout the catalytic cycle suggesting a tetrahedral localized carbanion rather than a planar enamine as reported for pyruvate oxidase and transketolase (*20, 42*). A localized carbanion would be a very strong base and will be immediately quenched by any available proximal proton source. This could explain why His281 is not invariant in BFDCs and may be replaced by Tyr, Ser, or Thr residues (*38*). A localized carbanion rather than a resonance-stabilized enamine has also been proposed for indolepyruvate decarboxylase and oxalyl-CoA decarboxylase (*8, 43*).

The structural studies on BFDC further confirm that the stereochemical course in ThDP enzymes is conserved with an identical stereochemistry at C2α and a three-center binding mode with specific interactions for the leaving group, the substrate carbonyl group, and the substrate substituent. The substrate leaving group is always directed perpendicular to the thiazolium ring plane, and the substrate carbonyl oxygen is in close proximity to the 4′-amino group of ThDP (*24*). Conforming with studies on other thiamin enzymes, the aminopyrimidine ring of tetrahedral ThDP intermediates is stabilized in the 1′,4′-imino tautomeric form (*10*). Finally, the active center of BFDC is found to be highly specific for binding and conversion of the native substrate BF. Modification of the phenyl ring (NBF) or replacement of the carboxylate by methylphosphonate (MBP) greatly impairs binding and turnover resulting in an intricate kinetic analysis.

SUPPORTING INFORMATION AVAILABLE

Initial omit and simulated annealing omit maps of PMThDP bound to BFDC, circular dichroism spectra after titration of MBP to BFDC, kinetics of PMThDP formation using NMR spectroscopy, and stereo drawing of the active center of BFDC including electron density maps of the final model. This material is available free of charge via the Internet at http://pubs.acs.org.

REFERENCES

1. Gunsalus, I. C., Gunsalus, C. F., and Stanier, R. Y. (1953) The enzymatic conversion of mandelic acid to benzoic acid. 1. Gross fractionation of the system into soluble and particulate components. *J. Bacteriol. 66*, 538–542.
2. Hegeman, G. D. (1966) Synthesis of enzymes of mandelate pathway by *Pseudomonas putida*. 1. Synthesis of enzymes by wild type. *J. Bacteriol. 91*, 1140–1154.
3. Hegeman, G. D. (1966) Synthesis of enzymes of mandelate pathway by *Pseudomonas putida*. 2. Isolation and properties of blocked mutants. *J. Bacteriol. 91*, 1155–1160.
4. Hegeman, G. D. (1966) Synthesis of enzymes of mandelate pathway by *Pseudomonas putida*. 3. Isolation and properties of constitutive mutants. *J. Bacteriol. 91*, 1161–1167.
5. Hegeman, G. D., Rosenberg, E. Y., and Kenyon, G. L. (1970) Mandelic acid racemase from *Pseudomonas putida*: Purification and properties of enzyme. *Biochemistry 9*, 4029–4036.
6. Ornston, L. N., and Stanier, R. Y. (1966) Conversion of catechol and protocatechuate to beta-ketoadipate by *Pseudomonas putida*. *J. Biol. Chem. 241*, 3776–3786.
7. Hegeman, G. D. (1970) Mandelate decarboxylase (*Pseudomonas putida*). *Methods Enzymol. 17*, 674–678.
8. Schütz, A., Golbik, R., König, S., Hübner, G., and Tittmann, K. (2005) Intermediates and transition states in thiamin diphosphate-dependent decarboxylases. A kinetic and NMR study on wild-type indolepyruvate decarboxylase and variants using indolepyruvate, benzoylformate, and pyruvate as substrates. *Biochemistry 44*, 6164–6179.
9. Kern, D., Kern, G., Neef, H., Tittmann, K., KillenbergJabs, M., Wikner, C., Schneider, G., and Hübner, G. (1997) How thiamine diphosphate is activated in enzymes. *Science 275*, 67–70.
10. Nemeria, N., Baykal, A., Joseph, E., Zhang, S., Yan, Y., Furey, W., and Jordan, F. (2004) Tetrahedral intermediates in thiamin diphosphate-dependent decarboxylations exist as a 1′,4 ′-imino tautomeric form of the coenzyme, unlike the Michaelis complex or the free coenzyme. *Biochemistry 43*, 6565–6575.
11. Nemeria, N., Chakraborty, S., Baykal, A., Korotchkina, L. G., Patel, M. S., and Jordan, F. (2007) The 1′,4 ′-iminopyrimidine tautomer of thiamin diphosphate is poised for catalysis in asymmetric active centers on enzymes. *Proc. Natl. Acad. Sci. U.S.A. 104*, 78–82.
12. Hasson, M. S., Muscate, A., McLeish, M. J., Polovnikova, L. S., Gerlt, J. A., Kenyon, G. L., Petsko, G. A., and Ringe, D. (1998) The crystal structure of benzoylformate decarboxylase at 1.6 angstrom resolution: Diversity of catalytic residues in thiamin diphosphate-dependent enzymes. *Biochemistry 37*, 9918–9930.
13. Arjunan, P., Umland, T., Dyda, F., Swaminathan, S., Furey, W., Sax, M., Farrenkopf, B., Gao, Y., Zhang, D., and Jordan, F. (1996) Crystal structure of the thiamin diphosphate-dependent enzyme pyruvate decarboxylase from the yeast *Saccharomyces cerevisiae* at 2.3 angstrom resolution. *J. Mol. Biol. 256*, 590–600.
14. Dobritzsch, D., König, S., Schneider, G., and Lu, G. G. (1998) High resolution crystal structure of pyruvate decarboxylase from *Zymomonas mobilis*—Implications for substrate activation in pyruvate decarboxylases. *J. Biol. Chem. 273*, 20196–20204.
15. Polovnikova, E. S., McLeish, M. J., Sergienko, E. A., Burgner, J. T., Anderson, N. L., Bera, A. K., Jordan, F., Kenyon, G. L., and Hasson, M. S. (2003) Structural and kinetic analysis of catalysis by a thiamin diphosphate-dependent enzyme, benzoylformate decarboxylase. *Biochemistry 42*, 1820–1830.
16. Sergienko, E. A., Wang, J., Polovnikova, L., Hasson, M. S., McLeish, M. J., Kenyon, G. L., and Jordan, F. (2000) Spectroscopic detection of transient thiamin diphosphate-bound intermediates on benzoylformate decarboxylase. *Biochemistry 39*, 13862–13869.
17. Kluger, R., and Moore, I. F. (2000) Destruction of vitamin B1 by benzaldehyde. Reactivity of intermediates in the fragmentation of N1′-benzyl-2-(1-hydroxybenzyl)thiamin. *J. Am. Chem. Soc. 122*, 6145–6150.
18. Kluger, R., and Pike, D. C. (1977) Active-site generated analogs of reactive intermediates in enzymic reactions: Potent inhibition of pyruvate-dehydrogenase by a phosphonate analog of pyruvate. *J. Am. Chem. Soc. 99*, 4504–4506.
19. Arjunan, P., Sax, M., Brunskill, A., Chandrasekhar, K., Nemeria, N., Zhang, S., Jordan, F., and Furey, W. (2006) A thiamin-bound, pre-decarboxylation reaction intermediate analogue in the pyruvate dehydrogenase E1 subunit induces large scale disorder-to-order transformations in the enzyme and reveals novel structural features in the covalently bound adduct. *J. Biol. Chem. 281*, 15296–15303.
20. Wille, G., Meyer, D., Steinmetz, A., Hinze, E., Golbik, R., and Tittmann, K. (2006) The catalytic cycle of a thiamin diphosphate enzyme examined by cryocrystallography. *Nat. Chem. Biol. 2*, 324–328.

21. Brandt, G. S., Nemeria, N., Chakraborty, S., McLeish, M. J., Yep, A., Kenyon, G. L., Petsko, G. A., Jordan, F., and Ringe, D. (2008) Probing the active center, of benzaldehyde lyase with substitutions and the pseudosubstrate analogue benzoylphosphonic acid methyl ester. *Biochemistry 47*, 7734–7743.
22. Bera, A. K., Polovnikova, L. S., Roestamadji, J., Widlanski, T. S., Kenyon, G. L., McLeish, M. J., and Hasson, M. S. (2007) Mechanism-based inactivation of benzoylformate decarboxylase, a thiamin diphosphate-dependent enzyme. *J. Am. Chem. Soc. 129*, 4120–4121.
23. Tittmann, K., Golbik, R., Uhlemann, K., Khailova, L., Schneider, G., Patel, M., Jordan, F., Chipman, D. M., Duggleby, R. G., and Hübner, G. (2003) NMR analysis of covalent intermediates in thiamin diphosphate enzymes. *Biochemistry 42*, 7885–7891.
24. Kluger, R., and Tittmann, K. (2008) Thiamin diphosphate catalysis: Enzymic and nonenzymic covalent intermediates. *Chem. Rev. 108*, 1797–1833.
25. Hallmann, G., and Hagele, K. (1963) Benzofuranderivate-tryptamin-, serotonin- und melatonin-analoga. *Justus Liebig's Ann. Chem. 662*, 147.
26. Cleland, W. W. (1975) Partition analysis and concept of net rate constants as tools in enzyme-kinetics. *Biochemistry 14*, 3220–3224.
27. Hasson, M. S., Muscate, A., Henehan, G. T. M., Guidinger, P. F., Petsko, G. A., Ringe, D., and Kenyon, G. L. (1995) Purification and crystallization of benzoylformate decarboxylase. *Protein Sci. 4*, 955–959.
28. Otwinowski, Z., and Minor, W. (1997) Processing of X-ray diffraction data collected in oscillation mode. *Methods Enzymol. 276A*, 307–326.
29. Vagin, A., and Teplyakov, A. (1997) MOLREP: an automated program for molecular replacement. *J. Appl. Crystallogr. 30*, 1022–1025.
30. Colloborative Computational Project No. 4 (1994) The CCP4 suite: programs for protein crystallography. *Acta Crystallogr., Sect. D: Biol. Crystallogr. 50*, 760–763.
31. Emsley, P., and Cowtan, K. (2004) Coot: model-building tools for molecular graphics. *Acta Crystallogr., Sect. D: Biol. Crystallogr. 60*, 2126–2132.
32. Tittmann, K., Vyazmensky, M., Hübner, G., Barak, Z., and Chipman, D. M. (2005) The carboligation reaction of acetohydroxyacid synthase II: Steady-state intermediate distributions in wild type and mutants by NMR. *Proc. Natl. Acad. Sci. U.S.A. 102*, 553–558.
33. Tittmann, K., Wille, G., Golbik, R., Weidner, A., Ghisla, S., and Hübner, G. (2005) Radical phosphate transfer mechanism for the thiamin diphosphate- and FAD-dependent pyruvate oxidase from *Lactobacillus plantarum*. Kinetic coupling of intercofactor electron transfer with phosphate transfer to acetyl-thiamin diphosphate via a transient FAD semiquinone/hydroxyethyl-ThDP radical pair. *Biochemistry 44*, 13291–13303.
34. Asztalos, P., Parthier, C., Golbik, R., Kleinschmidt, M., Hübner, G., Weiss, M. S., Friedemann, R., Wille, G., and Tittmann, K. (2007) Strain and near attack conformers in enzymic thiamin catalysis: X-ray crystallographic snapshots of bacterial transketolase in covalent complex with donor ketoses xylulose 5-phosphate and fructose 6-phosphate, and in noncovalent complex with acceptor aldose ribose 5-phosphate. *Biochemistry 46*, 12037–12052.
35. Berthold, C. L., Gocke, D., Wood, D., Leeper, F. J., Pohl, M., and Schneider, G. (2007) Structure of the branched-chain keto acid decarboxylase (KdcA) from *Lactococcus lactis* provides insights into the structural basis for the chemoselective and enantioselective carboligation reaction. *Acta Crystallogr., Sect. D: Biol. Crystallogr. 63*, 1217–1224.
36. Schütz, A., Sandalova, T., Ricagno, S., Hübner, G., König, S., and Schneider, G. (2003) Crystal structure of thiamindiphosphate-dependent indolepyruvate decarboxylase from *Enterobacter cloacae*, an enzyme involved in the biosynthesis of the plant hormone indole-3-acetic acid. *Eur. J. Biochem. 270*, 2312–2321.
37. Versees, W., Spaepen, S., Vanderleyden, J., and Steyaert, J. (2007) The crystal structure of phenylpyruvate decarboxylase from *Azospirillum brasilense* at 1.5 angstrom resolution-Implications for its catalytic and regulatory mechanism. *FEBS J. 274*, 2363–2375.
38. Yep, A., Kenyon, G. L., and McLeish, M. J. (2008) Saturation mutagenesis of putative catalytic residues of benzoylformate decarboxylase provides a challenge to the accepted mechanism. *Proc. Natl. Acad. Sci. U.S.A. 105*, 5733–5738.
39. Weiss, P. M., Garcia, G. A., Kenyon, G. L., Cleland, W. W., and Cook, P. F. (1988) Kinetics and mechanism of benzoylformate decarboxylase using C-13 and solvent deuterium-isotope effects on benzoylformate and benzoylformate analogs. *Biochemistry 27*, 2197–2205.
40. Albery, W. J., and Knowles, J. R. (1977) Efficiency and evolution of enzyme catalysis. *Angew. Chem., Int. Ed. Engl. 16*, 285–293.
41. Kluger, R., Ikeda, G., Hu, Q. Y., Cao, P. P., and Drewry, J. (2006) Accelerating unimolecular decarboxylation by preassociated acid catalysis in thiamin-derived intermediates: Implicating Bronsted acids as carbanion traps in enzymes. *J. Am. Chem. Soc. 128*, 15856–15864.
42. Fiedler, E., Thorell, S., Sandalova, T., Golbik, R., König, S., and Schneider, G. (2002) Snapshot of a key intermediate in enzymatic thiamin catalysis: Crystal structure of the alpha-carbanion of (alpha,beta-dihydroxyethyl)-thiamin diphosphate in the active site of transketolase from *Saccharomyces cerevisiae*. *Proc. Natl. Acad. Sci. U.S.A. 99*, 591–595.
43. Berthold, C. L., Toyota, C. G., Moussatche, P., Wood, M. D., Leeper, F., Richards, N. G. J., and Lindqvist, Y. (2007) Crystallographic snapshots of oxalyl-CoA decarboxylase give insights into catalysis by nonoxidative ThDP-dependent decarboxylases. *Structure 15*, 853–861.

BI801957D